

Article

Thermal Onsets of Viscous Dissipation for Radiative Mixed Convective Flow of Jeffery Nanofluid across a Wedge

Yogesh Dadhich ¹, Nazek Alessa ^{2,*}, Reema Jain ^{1,*}, Abdul Razak Kaladgi ³, Karuppusamy Loganathan ¹ and V. Radhika Devi ⁴

- ¹ Department of Mathematics and Statistics, Manipal University Jaipur, Jaipur 303007, Rajasthan, India
² Department of Mathematical Sciences, College of Sciences, Princess Nourah Bint Abdulrahman University, P.O. Box 84428, Riyadh 11671, Saudi Arabia
³ Department of Mechanical Engineering, P. A. College of Engineering (Affiliated to Visvesvaraya Technological University, Belagavi), Mangaluru 574153, Karnataka, India
⁴ Department of Science and Humanities, MLR Institute of Technology, Hyderabad 500043, Telangana, India
* Correspondence: nazekaa@yahoo.com (N.A.); reemajain197@gmail.com (R.J.)

Abstract: The current analysis discusses Jeffery nanofluid's thermally radiative flow with convection over a stretching wedge. It takes into account the Brownian movement and thermophoresis of the Buongiorno nanofluid model. The guiding partial differential equations (PDEs) are modified by introducing the symmetry variables, leading to non-dimensional ordinary differential equations (ODEs). To solve the generated ODEs, the MATLAB function `bvp4c` is implemented. Examined are the impacts of different flow variables on the rate of transmission of heat transfer (HT), temperature, mass, velocity, and nanoparticle concentration (NC). It has been noted that the velocity and mass transfer were increased by the pressure gradient factor. Additionally, the thermal boundary layer (TBL) and nanoparticle concentration are reduced by the mixed convection (MC) factor. In order to validate the present research, the derived numerical results were compared to previous findings from the literature while taking into account the specific circumstances. It was found that there was good agreement in both sets of data.



Citation: Dadhich, Y.; Alessa, N.; Jain, R.; Kaladgi, A.R.; Loganathan, K.; Devi, V.R. Thermal Onsets of Viscous Dissipation for Radiative Mixed Convective Flow of Jeffery Nanofluid across a Wedge. *Symmetry* **2023**, *15*, 385. <https://doi.org/10.3390/sym15020385>

Academic Editors: Jan Awrejcewicz and Sergei D. Odintsov

Received: 3 October 2022

Revised: 29 January 2023

Accepted: 30 January 2023

Published: 1 February 2023



Copyright: © 2023 by the authors. Licensee MDPI, Basel, Switzerland. This article is an open access article distributed under the terms and conditions of the Creative Commons Attribution (CC BY) license (<https://creativecommons.org/licenses/by/4.0/>).

Keywords: Jeffery nanofluid; symmetry variables; wedge; viscous dissipation; radiation effect; Brownian motion; mass transfer

1. Introduction

Non-Newtonian transport phenomena can be found in a large number of scientific domains such as mechanical, biochemical, and materials science. The momentum conservation equations are usually modified in certain ways in non-Newtonian models. These include tangent hyperbolic liquids, power-law fluids, Oldroyd-B systems, Reiner-Rivlin systems, Walters-B short memory systems, and Bingham polymers [1–9]. The Jeffrey model has shown to be quite successful, just like many other rheological models that have been constructed. This beautiful yet simple rheological model was initially developed to represent issues with flow in the earth's crust [10]. This model [11] is a viscoelastic fluid model that displays strong shear viscosity, yield stress, and shear thinning features. When the wall stress is significantly higher than the yield stress, the Jeffrey fluid model degenerates to a Newtonian fluid. The rheological behavior of various liquids, such as physiological suspensions, foams, geological materials, cosmetics, and syrups, is also approximated by this fluid model fairly well. Jeffery fluid flow with a range of viscosities [12], Jeffery fluid radiative transfer with a heat source [13], as well as the latest research on Jeffery fluid [14–16], are also fairly well taken. It is important to analyze the HT of BL flow involving thermal radiation (R) in a number of production processes, including extreme temperature solar, glass production, and liquid metals. These transport mechanism issues turn out to be incredibly nonlinear when combined with convection processes.

Numerous studies that consider radiative-convective flow in multiple physical dimensions have been carried out. Ara et al. [17] examined how radiation affected the BL flow of a gradually declining Powell fluid sheet. They found a diminution in the BL, with a rise in radiation and Prandtl number Pr . With the use of the Rosseland exemplary, Noor NF et al. [18] examined the impact of R on magneto-hydrodynamics (MHD) with thermophoresis down an angled plate. Additionally, radiation, along with convection, in a Micropolar Shrinking Sheet was investigated by Gupta et al. [19]. The physical characteristics of a MHD Carreau nanofluid bi-convection flow across an upper paraboloid porous surface are examined by Shahid et al. [20]. Chemical reactions and the presence of activation energy are both investigated in this study. Bhargava et al. [21] investigated convective effects of micropolar fluid with TR in a porous medium. The Falkner–Skan flow was only partially considered in earlier studies [22,23]. The 2D wedge structure is connected to this class of BL flows. Peddieson [24] employed the second-order Rivlin model to explain how non-Newtonian flows through wedges develop. Researchers are interested in understanding more about the mixed convection (MC) BL flow over a wedge as it has many applications in engineering systems. Sparrow et al. [25] were among the first to investigate the MC convection flow and HT around a non-isothermal wedge with a non-uniform velocity. The flow of MC with constant injection or suction across a porous wedge was investigated by Watanabe et al. [26]. By using a wedge, Kafoussias [27] and Nanousis [28] looked into the effects of injection and suction on MC Flow. A power-law model was used by Gorla [29] to examine HT in a flow via a wedge. Yih [30] investigated how radiation affected the flow of MC around a wedge immersed in porous media. For a third-grade flow generated by a non-isothermal wedge, Rashidi et al. [31] used a homotopy approach. The calculations for MHD forced convection flow across a wedge were determined by Chamkha et al. [32] using a finite difference approach. MHD convection through a porous wedge was examined by Hsiao [33], who found an increment in the HT rates with increases in R and Pr . In a non-Newtonian flow, Ishak et al. [34] investigated mathematically the 2D, laminar flow across a wedge. Dadhich et al. [35] investigated the MHD flow of Sisko fluid across a wedge. For infinite shear rate, Khan et al. [36] investigated the effects of various factors of Carreau flow across a wedge.

Nanotechnology is the strategy of investigating and isolating or adding an item's particles and atoms that should be made tiny. Nanomaterials has had a substantial impact on a wide range of initiatives over the past thirty years, such as the oil industry, food production, medicine, nuclear energy, nuclear cooling, and the polymer firm. In order to improve the heat transfer performance of a nanofluid utilizing thermomagnetic convection, Prabhakaran et al. [37] inspect the consequence of MHD mixed convective flow of CNTs/ Al_2O_3 nanofluid in water past a heated stretchy plate with injection/suction, heat consumption and radiation. Du et al. [38] explored a modified model based on the Buongiorno model that took into account the Kelvin force in the presence of an inhomogeneous magnetic field. Wang et al. [39] used numerical simulations to study the EHD effect for various electrode configurations, electric field intensities, and frequency ranges. Sharma et al. [40] examined an incompressible electrically conducting viscous fluid in the presence of heat radiation, viscous dissipation, a first-order chemical reaction with thermophoresis, and Brownian motion across a constantly expanding surface. The fluid flow zone is subjected to an inclined uniform magnetic field. A few cutting-edge research reports have been gathered in Refs. [41–44].

Given the above-mentioned literature, we observed that no investigation has been carried out to examine the combined convection of heat and mass transmission in Jeffery fluid across a wedge with heat production and radiation with Joule heating. To fill the space in the existing analysis we studied Jeffery fluid across a wedge. By adding the necessary similarity variables, the guiding partial differential equations (PDEs) are adjusted, resulting in non-dimensional ordinary differential equations (ODEs). The numerical solution has been obtained by the BVP4c method. The impact of velocity, temperature, and concentration are manifested as graphs. The current issue, which has application to the simulation of

nuclear waste and polymeric manufacturing processes, but has not yet been documented in the scientific literature, is known to the authors.

2. Computational Modelling

In this work, 2D, steady, laminar flow of Jeffery nanofluid with radiation and a heat source is investigated. It is presented in Figure 1 using a rectangular coordinate system. The wedge surface is parallel to and perpendicular to the coordinate axes, and the free stream velocity is $u_\infty(x) = Px^m$ ($P > 0$). The wedge angle is $\Omega = \pi \beta_1$, where $\beta_1 = \frac{2m}{m+1}$. It is also supposed that the nanoparticle fraction C and temperature T take constant values of C_w and T_w , respectively, on the wedge surface. T_∞ and C_∞ , respectively, are the surrounding values for y tending to ∞ . Transverse to the wedge surface is an imposed uniform magnetic field (B_0). Mathematical model for the flow analysis is presented in Figure 1.

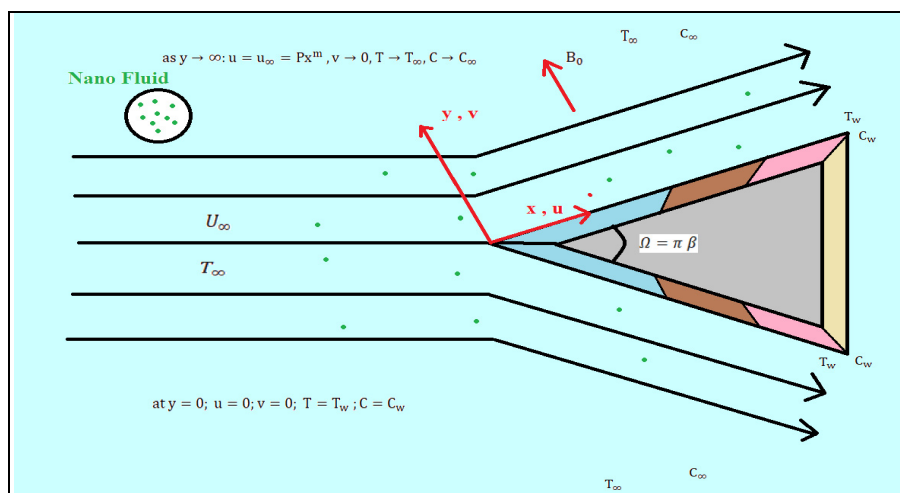


Figure 1. Mathematical model for the current analysis.

A non-Newtonian fluid described by Jeffreys [45] has the Cauchy stress tensor, S , with the following form:

$$T = -pI + S, S = \frac{\mu}{1 + \lambda_1} (\dot{\gamma} + \lambda_2 \ddot{\gamma}),$$

where $\dot{\gamma}$ is the shear rate; a dot above a quantity indicates the material time derivative. An elegant approach for modelling the retardation and relaxation effects that arise in non-Newtonian polymer flows is provided by the Jeffreys model. In terms of the velocity vector, V , the shear rate and gradient of the shear rate are further defined as follows:

$$\dot{\gamma} = \nabla V + (\nabla V)^T;$$

$$\ddot{\gamma} = \frac{d}{dt}(\dot{\gamma}).$$

For a 2D Jeffery fluid, the governing BL equations, which are the equations of continuity, momentum, and energy, are given as follows [15]:

$$\frac{\partial u}{\partial x} + \frac{\partial v}{\partial y} = 0; \tag{1}$$

$$u \frac{\partial u}{\partial x} + v \frac{\partial u}{\partial y} = u_\infty \frac{du_\infty}{dx} + \frac{\sigma}{1 + \lambda_1} \left[\frac{\partial^2 u}{\partial y^2} + \lambda_2 \left(u \frac{\partial^3 u}{\partial x \partial y^2} + v \frac{\partial^3 u}{\partial y^3} - \frac{\partial u}{\partial x} \frac{\partial^2 u}{\partial y^2} + \frac{\partial u}{\partial y} \frac{\partial^2 u}{\partial x \partial y} \right) \right] - \frac{\sigma B_0^2 u}{\rho_f} + g\beta(T - T_\infty) \sin\left(\frac{\Omega}{2}\right) + g\beta^*(C - C_\infty) \sin\left(\frac{\Omega}{2}\right); \tag{2}$$

$$u \frac{\partial T}{\partial x} + v \frac{\partial T}{\partial y} = \frac{k}{(\rho C_p)_f} \frac{\partial^2 T}{\partial y^2} + \tau \left[D_B \frac{\partial C}{\partial y} \frac{\partial T}{\partial y} + \frac{D_T}{T_\infty} \left(\frac{\partial T}{\partial y} \right)^2 \right] - \frac{1}{(\rho C_p)_f} \frac{\partial q_r}{\partial y} + \frac{Q}{(\rho C_p)_f} (T - T_\infty) + \frac{\mu}{(\rho C_p)_f} \left(\frac{\partial u}{\partial y} \right)^2 + \frac{\sigma B_0^2 u^2}{(\rho C_p)_f}; \tag{3}$$

$$u \frac{\partial C}{\partial x} + v \frac{\partial C}{\partial y} = D_B \frac{\partial^2 C}{\partial y^2} + \frac{D_T}{T_\infty} \frac{\partial^2 T}{\partial y^2}. \tag{4}$$

ρ indicates the nanofluid particle material density, $\tau = \frac{(\rho C_p)_p}{(\rho C_p)_f}$ denotes the shear stress, D_B signifies the Brownian diffusion coefficient, D_T denotes the thermophoresis diffusion coefficient, q_r represents the radiative heat flux, and $\frac{k}{(\rho C_p)_f} = \alpha_f$ represents thermal diffusivity.

The related BCs are the following:

$$\text{at } y = 0 : u = 0, v = 0, T = T_w, C = C_w;$$

$$\text{as } y \rightarrow \infty : u = u_\infty = Px^m, v \rightarrow 0, T \rightarrow T_\infty, C \rightarrow C_\infty. \tag{5}$$

A stream function ψ is used to satisfy the equation of continuity such that $u = \frac{\partial \psi}{\partial y}$ and $v = -\frac{\partial \psi}{\partial x}$. The aforementioned BCs and equations are obtained in their non-dimensional form by using the accompanying similarity transformations.

The following symmetry variables transformation was used:

$$\eta = \sqrt{\left(\frac{m+1}{2}\right) \frac{(x)^{m-1}}{\vartheta}} y;$$

$$u = k(x)^m f'(\eta);$$

$$v = -\sqrt{\left(\frac{m+1}{2}\right) \vartheta k(x)^{m-1} \left[f(\eta) + \eta \left(\frac{m-1}{m+1}\right) f'(\eta) \right]};$$

$$\theta(\eta) = \frac{T - T_\infty}{T_w - T_\infty};$$

$$\Phi(\eta) = \frac{C - C_\infty}{C_w - C_\infty}. \tag{6}$$

The Rosseland diffusion flux model is defined as

$$q_r = -\frac{4\sigma^*}{3k^*} \frac{\partial T^4}{\partial y}. \tag{7}$$

The symbols k^* and σ^* represent the Stefan-Boltzmann constant and the mean absorption coefficient of Rosseland, respectively. T^4 can be described as a linear function of temperature by making the assumption that the temperature changes within the flow are negligibly small [9,20].

$$T^4 = 4T_\infty^3 - 3T_\infty^4. \tag{8}$$

Equations (7) and (8) are used in Equation (3) to produce

$$\frac{\partial q_r}{\partial y} = -\frac{16\sigma^* T_\infty^3}{3k^*} \frac{\partial^2 T}{\partial y^2}.$$

Equation (6) is incorporated into Equation (2) through (5) to produce the nonlinear ODE system shown below:

$$\left(\frac{m+1}{2}\right)f''' + \beta\left\{f'f'''(m-1) + f''^2\left(\frac{3m-1}{2}\right) - ff''''\left(\frac{m+1}{2}\right)\right\} - (1 + \lambda_1)\left\{mf'^2 - ff''\left(\frac{m+1}{2}\right)\right\} - M(1 + \lambda_1)f + m(1 + \lambda_1) + \lambda\{\theta + N\Phi\}\sin\left(\frac{\Omega}{2}\right) = 0; \quad (9)$$

$$\left(1 + \frac{4R}{3}\right)\theta'' + \text{Pr}(f\theta' + N_b\theta'\phi' + N_t\theta'^2) + \frac{2}{(m+1)}\delta\text{Pr}\theta + \text{MPr}E_c f^2 + E_c f''^2 = 0; \quad (10)$$

$$\Phi'' + \text{Pr}L_e f\Phi' + \left(\frac{N_t}{N_b}\right)\theta'' = 0; \quad (11)$$

$$\text{at } \eta = 0: f(\eta) = 0, f'(\eta) = 0, \theta(\eta) = 1, \Phi(\eta) = 1; \quad (12)$$

$$\text{as } \eta \rightarrow \infty: f'(\eta) = 1, f(\eta) = 1, \theta(\eta) = 0, \Phi(\eta) = 0. \quad (13)$$

The “prime” denotes the differentiation with respect to η , while the dimensionless terms are defined as the following:

$M = \frac{\sigma B_0^2 x}{\rho u_\infty} = \frac{kg^{-1}s^3 A^2 m^{-1} kg^2 s^{-4} A^{-2} m}{kg m^{-2} s^{-1}} = Constant$	Magnetic field factor
$P_r = \frac{\mu}{\alpha_f}$	Prandtl number
$N_b = \frac{\tau D_B (C_w - C_\infty)}{\theta}$	Brownian motion factor
$N_t = \frac{\tau D_T (T_w - T_\infty)}{\theta T_\infty}$	Thermophoresis factor
$L_e = \frac{\alpha_f}{D_B}$	Lewis number
$R = \frac{4\sigma^* T_\infty^3}{k^* k}$	Radiation factor
$\delta = \frac{Qx}{\rho c_p u_\infty} = \frac{kg m^2 s^{-3} m^{-3} k^{-1} m}{kg m^{-1} s^{-2} k^{-1} m s^{-1}} = Constant$	Source/sink factor
$E_c = \frac{(u_\infty)^2}{(c_p)_f (T_w - T_\infty)}$	Eckert number
$N = \frac{\beta^* (C_w - C_\infty)}{\beta (T_w - T_\infty)}$	Concentration to thermal buoyancy ratio factor
$\lambda = \frac{G_{rx}}{(R_{ex})^2}$	Mixed convection factor
$G_{rx} = \frac{g\beta(T_w - T_\infty)x^3}{4\theta^2} = \frac{m^4 s^{-2}}{4m^4 s^{-2}} = Constant$	Grashof number
$\beta = \frac{\lambda_2 u_\infty}{x} = \frac{sm s^{-1}}{m} = Constant$	Deborah number

Heat and Mass Transport Coefficients

The primary objective of this research is to determine those characteristics which are significant while dealing with heat and nanoparticle mass transportation processes.

These are described as the local Nusselt number $Nu_x = \left(\frac{xq_w}{k(T_w - T_\infty)}\right)_{y=0}$ and the local nanofluid Sherwood number $Sh_x = \left(\frac{xq_w}{D_B(C_w - C_\infty)}\right)_{y=0}$, where $q_w = -k\left(\frac{\partial T}{\partial y}\right)_{y=0}$ is the wall heat flux. As a result of the transformations mentioned above, these parameters will be reduced to $(Re_b)^{\frac{-1}{(m+1)}} Nu_x = -\left(1 + \frac{4R}{3}\right)\theta'(0)$ and $(Re_b)^{\frac{-1}{(m+1)}} Sh_x = -\phi'(0)$, respectively.

3. Numerical Computation

The approximate solutions with the BCs in Equations (12) and (13) for the nonlinear ODEs in Equations (9)–(11) are derived using the bvp4c MATLAB solver. The Equations set (9)–(13) is converted into a group of first-order DEs in Equations (14)–(26), as stated below, to execute the bvp4c coding:

$$f = y_1; \quad (14)$$

$$f' = y_1' = y_2; \quad (15)$$

$$f'' = y_2' = y_3; \quad (16)$$

$$f''' = y_3' = y_4; \quad (17)$$

$$\theta' = y_5' = y_6; \quad (18)$$

$$y'_6 = \theta''; \tag{19}$$

$$y'_7 = y_8 = \phi'; \tag{20}$$

$$y'_8 = \phi''; \tag{21}$$

$$f'''' = y_4' = \frac{y_4 \left(\frac{m+1}{2} \right) - M(1+\lambda_1)y_2 - (1+\lambda_1) \left[m(y_2)^2 - y_1 y_3 \left(\frac{m+1}{2} \right) \right] + \beta \left\{ y_2 y_4 (m-1) + (y_3)^2 \left(\frac{3m-1}{2} \right) \right\} + M(1+\lambda_1) + \lambda \{ y_4 + N y_6 \} \sin \frac{\Omega}{2}}{\beta y_1 \left(\frac{m+1}{2} \right)}; \tag{22}$$

$$\theta'' = y_6' = \frac{- \left[\left(\frac{2}{m+1} \right) \delta Pr y_5 + M Pr E_c y_2^2 + Pr (y_1 y_6 + N_b y_6 y_8 + N_t y_6^2) + E_c y_3^2 \right]}{\left(1 + \frac{4R}{3} \right)}; \tag{23}$$

$$y_8' = \phi'' = \frac{N_t \left[\left(\frac{2}{m+1} \right) \delta Pr y_5 + M Pr E_c y_2^2 + Pr (y_1 y_6 + N_b y_6 y_8 + N_t y_6^2) + E_c y_3^2 \right] - \left(1 + \frac{4R}{3} \right) Pr L_c N_b y_1 y_8}{N_b \left(1 + \frac{4R}{3} \right)}; \tag{24}$$

with the BCs:

$$y_0(1) = 0, \quad y_0(2) = 0, \quad y_0(5) - 1 = 0, \quad y_0(7) - 1 = 0; \tag{25}$$

$$y_1(2) = 0, \quad y_1(3) - 1 = 0, \quad y_1(5) = 0, \quad y_1(7) = 0. \tag{26}$$

4. Results and Discussion

4.1. λ_1 Impact on the Profiles of Velocity, Temperature, and Nanofluid Concentration (NC)

Figure 2a–c display the velocity, temperature, and NC patterns by altering the numerical values of λ_1 . The velocity is seen to increase with an increase in λ_1 . However, both the temperature and the concentration considerably drop. Through the buoyancy term, the mixed convection parameter connects the energy field and momentum field. This factor significantly affects the velocity, temperature, and concentration interactions while being a first-order factor. A thermal energy deficit brought on by the assistive buoyancy force’s momentum increase, cools the BL, and lowers its temperature and NC.

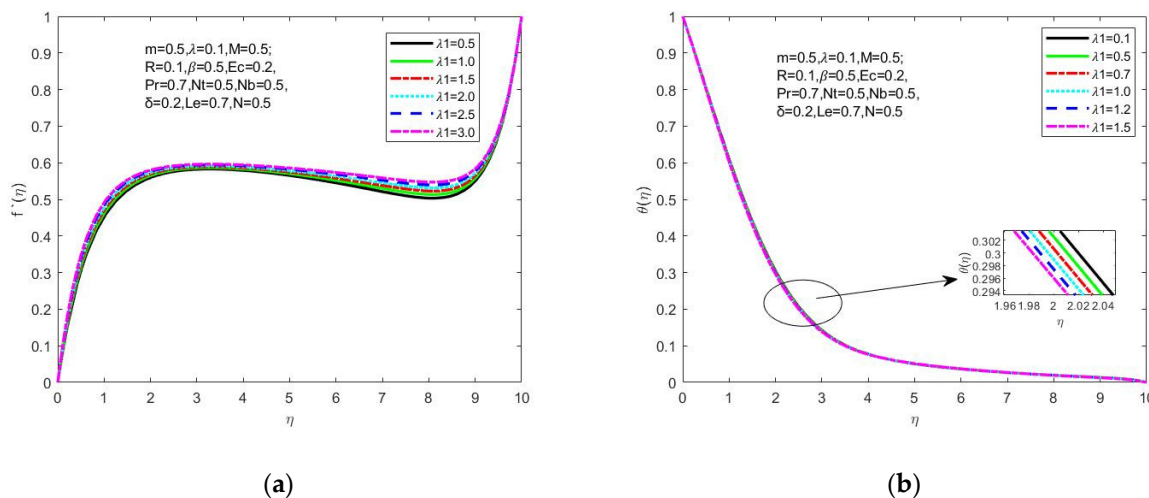
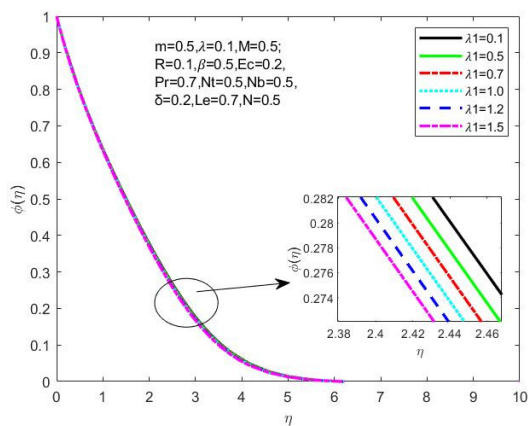


Figure 2. Cont.

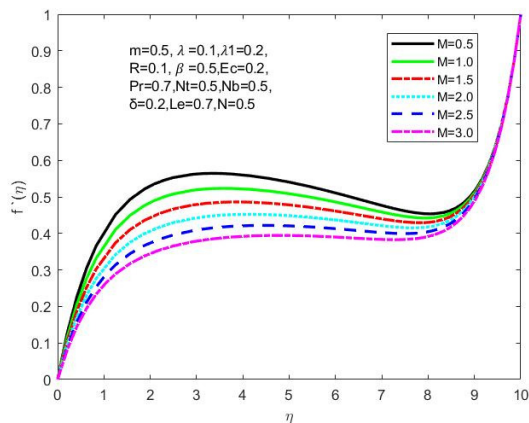


(c)

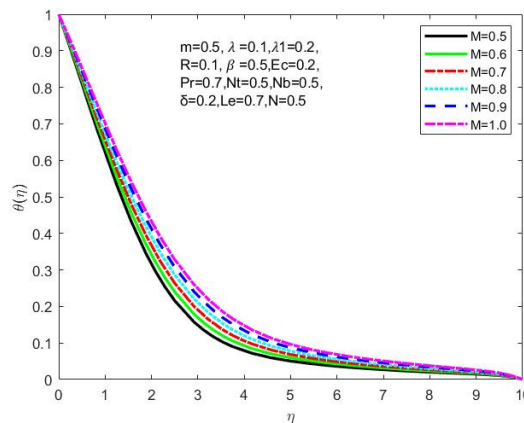
Figure 2. (a) f' vs. λ_1 , (b) θ vs. λ_1 , and (c) Φ vs. λ_1 .

4.2. Impact of M on Velocity, Temperature, and NC Profiles

Figure 3a–c illustrates the distributions of velocity, temperature, and NC by altering the numerical values of M . Figure 3a demonstrates that the nanofluid’s velocity reduces as the M value is raised while holding the other parameters constant. As M rises, so does the corresponding momentum BL thickness. Physically speaking, it makes sense that a greater M value would be able to reduce the speed of the fluid elements because the Lorentz force serves as a retarding force. Figure 3b,c show that as the magnetic parameter is increased within the BL region, both the temperature and concentrations are increased. The reason is that as the magnetic field intensity grows, the Lorentz force (a type of resistive force) also increases. As a result, the fluid’s temperature rises since more heat is produced there. Additionally, the TBL thicknesses show a similar pattern with a greater M value.

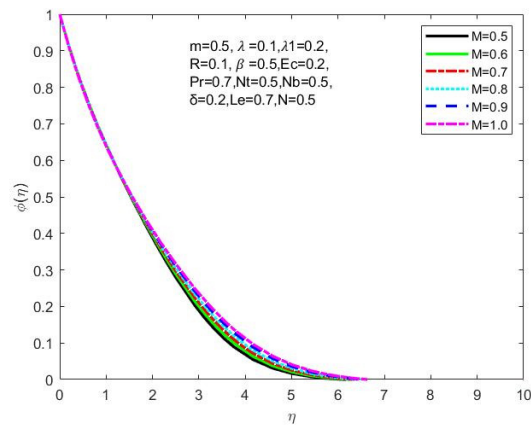


(a)



(b)

Figure 3. Cont.

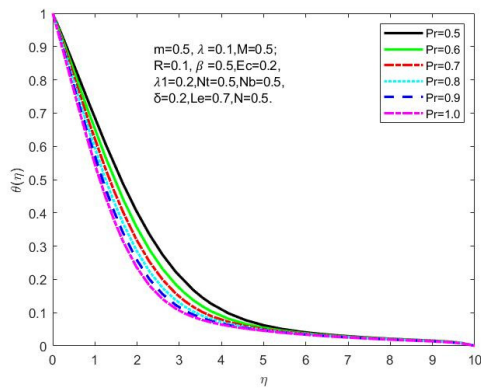


(c)

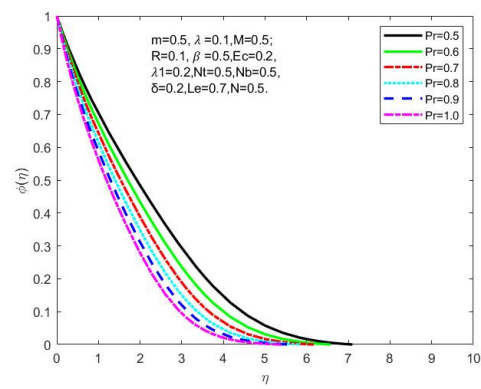
Figure 3. (a) f' vs. M , (b) θ vs. M , and (c) Φ vs. M .

4.3. Influence of Pr on Temperature, Concentration, and Velocity Patterns of the Nanofluids

Figure 4a–c shows how the Pr value affects the dispersion of heat, nanoparticle concentrations, and velocity. These graphs clearly show that a rise in Pr leads to a fall in fluid temperature since the strong momentum transport and low thermal diffusivity are demonstrated by high Pr . Due to its low heat dispersion and strong momentum transport, a fluid with a high Pr has a higher convective HT and a lower conductive HT. As a result, both the fluid’s temperature and its concentration of nanofluids fall, while the fluid’s velocity rises as momentum is transported with greater Pr .

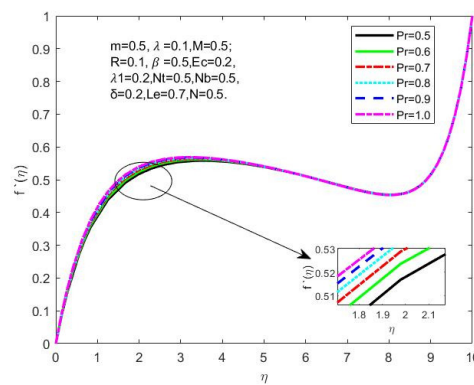


(a)



(b)

Figure 4. Cont.

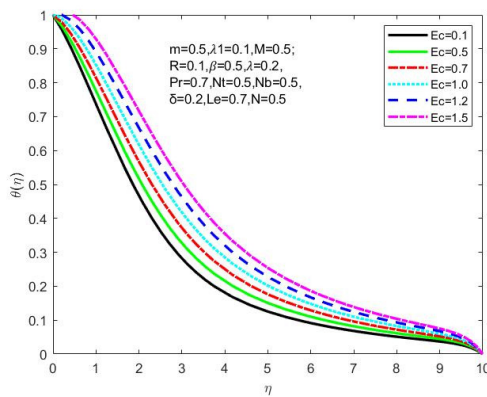


(c)

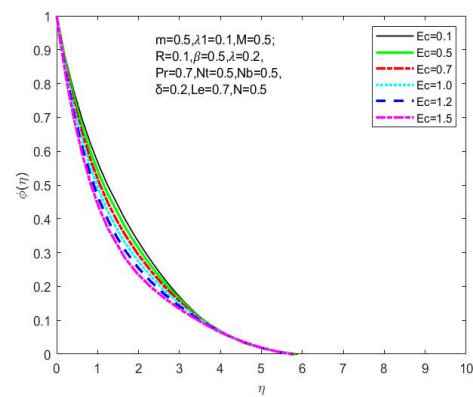
Figure 4. (a) θ vs. Pr , (b) Φ vs. Pr , and (c) f' vs. Pr .

4.4. Effect of Ec on Temperature, Concentration, and Velocity Profiles of the Nanofluids

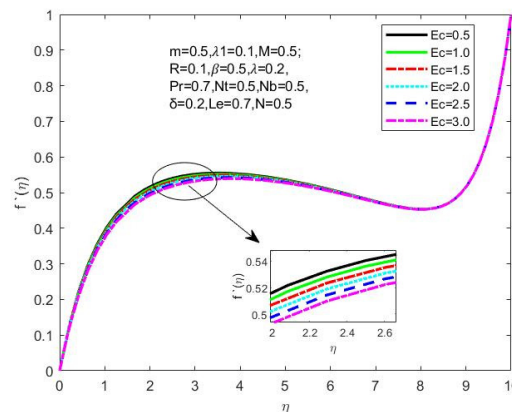
Figure 5a shows how the temperature changes as the Eckert number Ec varies. Ec is an assessment of the conversion of kinetic energy to heat via viscous dispersion. A boost in Ec results in an increase in temperature because heat is accumulated in nanofluid due to frictional heating. While, as seen in Figure 5b, the concentration of nanoparticles drops as the Eckert number rises. The velocity profile in Figure 5c exhibits the same pattern.



(a)



(b)



(c)

Figure 5. (a) f' vs. Ec , (b) θ vs. Ec , and (c) Φ vs. Ec .

4.5. Impact of N_b on Velocity, Temperature, and Concentration Patterns of the Nanofluids

Figure 6a–c show how N_b affects the velocity, temperature, and concentration curves. As N_b rises, the velocity in the BL drops. The volume fraction patterns of nanoparticles, however, decline. Through the direct transfer of thermal energy by the nanoparticles or indirectly through the micro-convection of fluid adjacent to the nanoparticles, the nanoparticle's Brownian motion has the potential to boost thermal transmission.

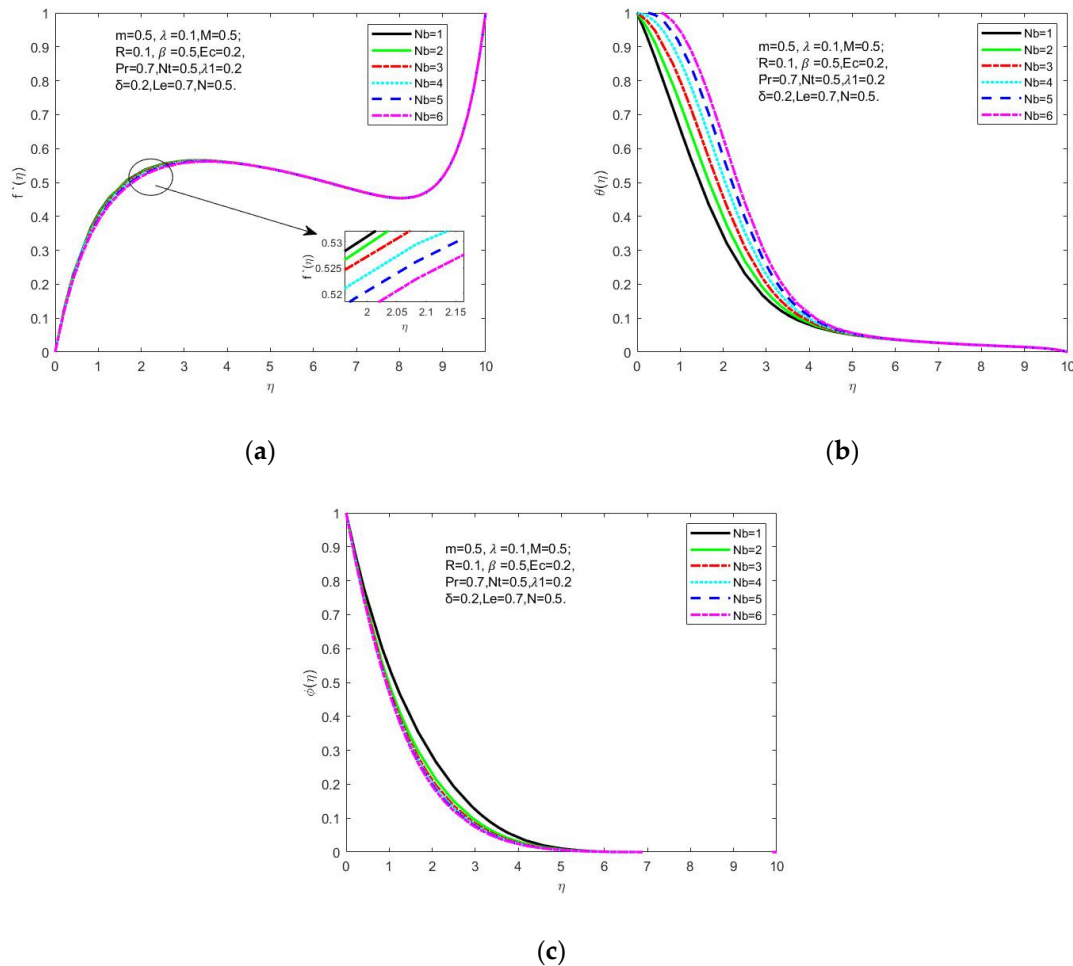


Figure 6. (a) f' vs. N_b , (b) θ vs. N_b , and (c) Φ vs. N_b .

4.6. Effect of δ Temperature, Concentration, and Velocity Profiles of the Nanofluids

The heat transport in fluid is significantly impacted by $\delta > 0$. The temperature upsurges, as depicted in Figure 7a–c. The enormous amount of heat energy generated in fluid elements escalates the thickness of the BL. This raises the thermal boundary's temperature. However, the concentration and velocity of the nanofluid drops with a rise in δ .

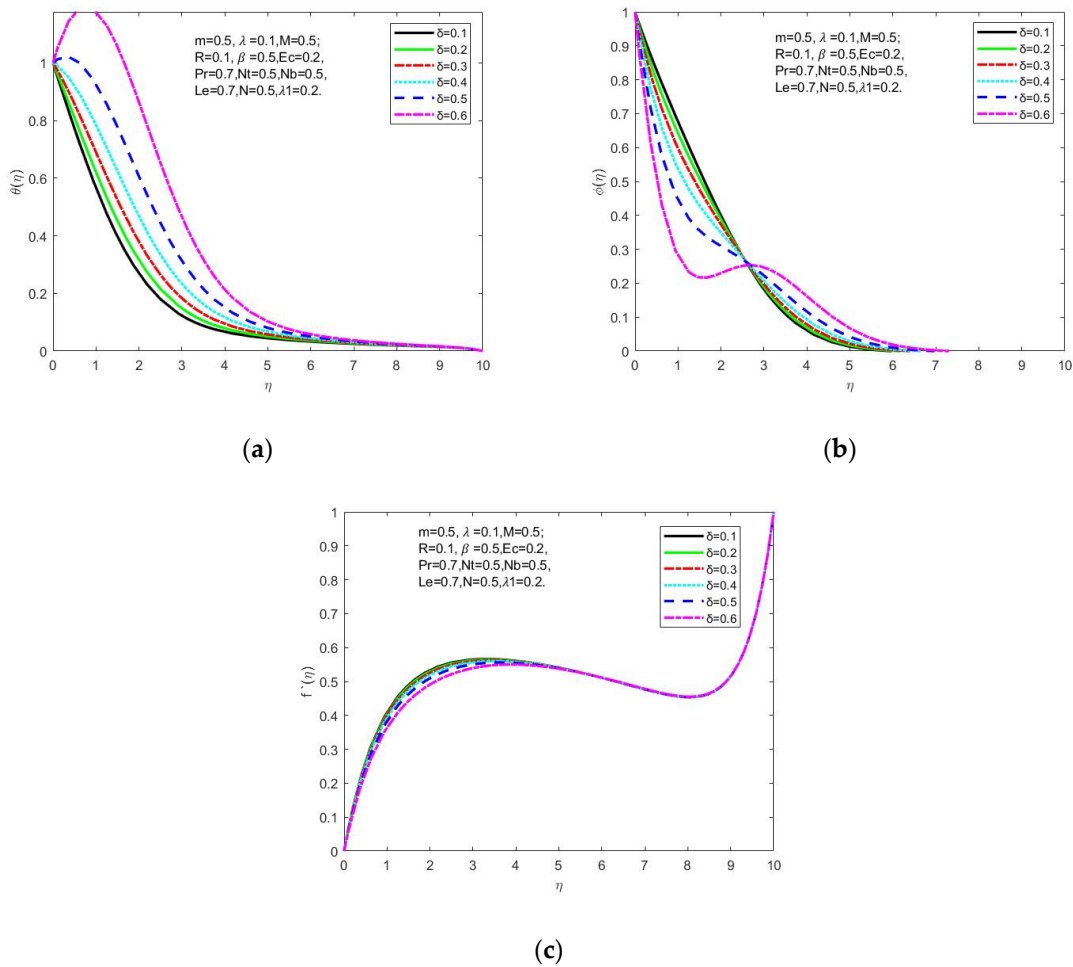


Figure 7. (a) θ vs. δ , (b) Φ vs. δ , and (c) f' vs. δ .

4.7. Impact of N on Concentration, Velocity, and Temperature Patterns of the Nanofluids

Figure 8a–c depicts how N affects the concentration, velocity, and temperature patterns of the nanofluids. It is clear that a rise in N leads to a rise in Φ . Obviously, when the Φ rises, the velocity reduces and hence the temperature rises as a result of less HT due to the low velocity of the nanofluids.

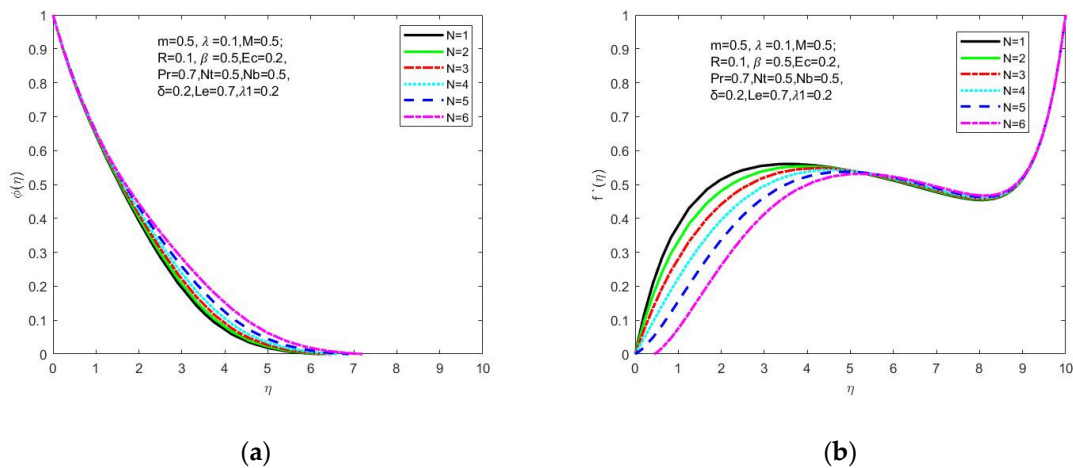
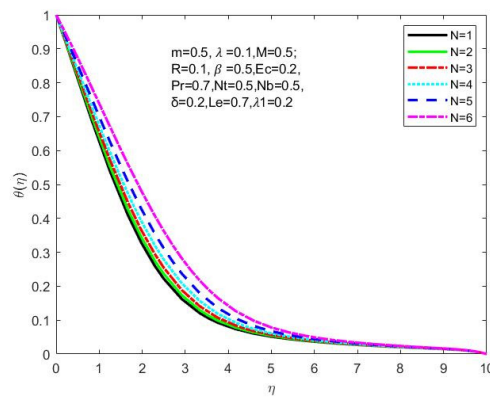


Figure 8. Cont.

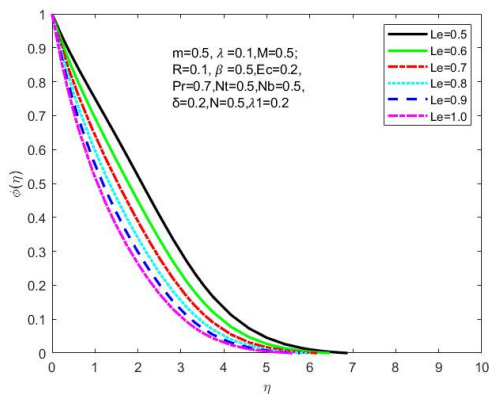


(c)

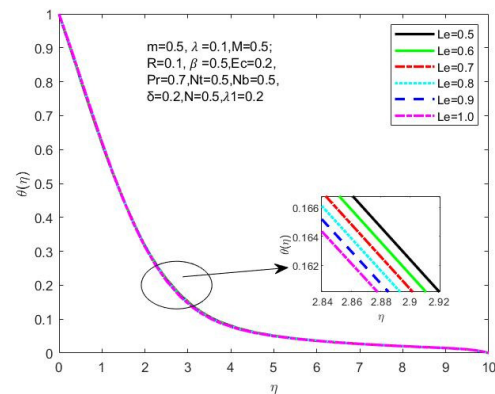
Figure 8. (a) f' vs. N , (b) θ vs. N , and (c) Φ vs. N .

4.8. Influence of Le on the Concentration, Velocity, and Temperature Profiles of the Nanofluids

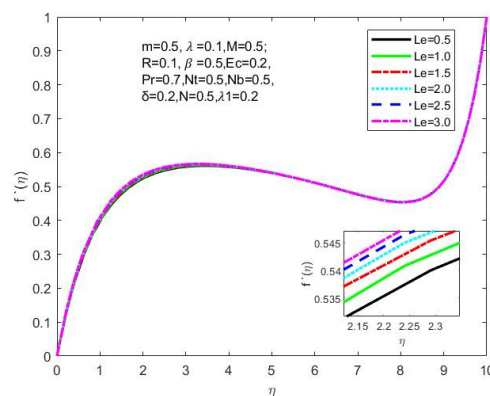
The variation of Le with Φ is shown in Figure 9a. It is obvious that Φ falls as Le increases. This is because D_b , which is associated with N_b , and Le have inversely proportionate relationships. The increase in Le thus causes the boundary layer's thermal diffusivity to decrease, which causes the speed in the boundary layer area to decrease. Similar variation was seen for the temperature profiles. On the other hand, there is an increment in velocity profiles for rising Le (See Figure 9b,c).



(a)



(b)



(c)

Figure 9. (a) Φ vs. Le , (b) θ vs. Le , and (c) f' vs. Le .

4.9. Impact of N_t on Fluid Velocity, Concentration, and Temperature Patterns of the Nanofluids

Figure 10a–c portray the characteristic patterns for velocity, temperature, and NC for different N_t values. It has been found that a rise in N_t causes a fall in velocity. At intermediate distances from the wedge, profile variations become more noticeable. However, raising N_t results in a significant improvement in both the temperature and NC values. Thermophoresis successfully heats the BL while assisting particle accumulation ahead of the fluid regime (on the wedge), which explains the increased concentrations of nanoparticles in Figure 10c.

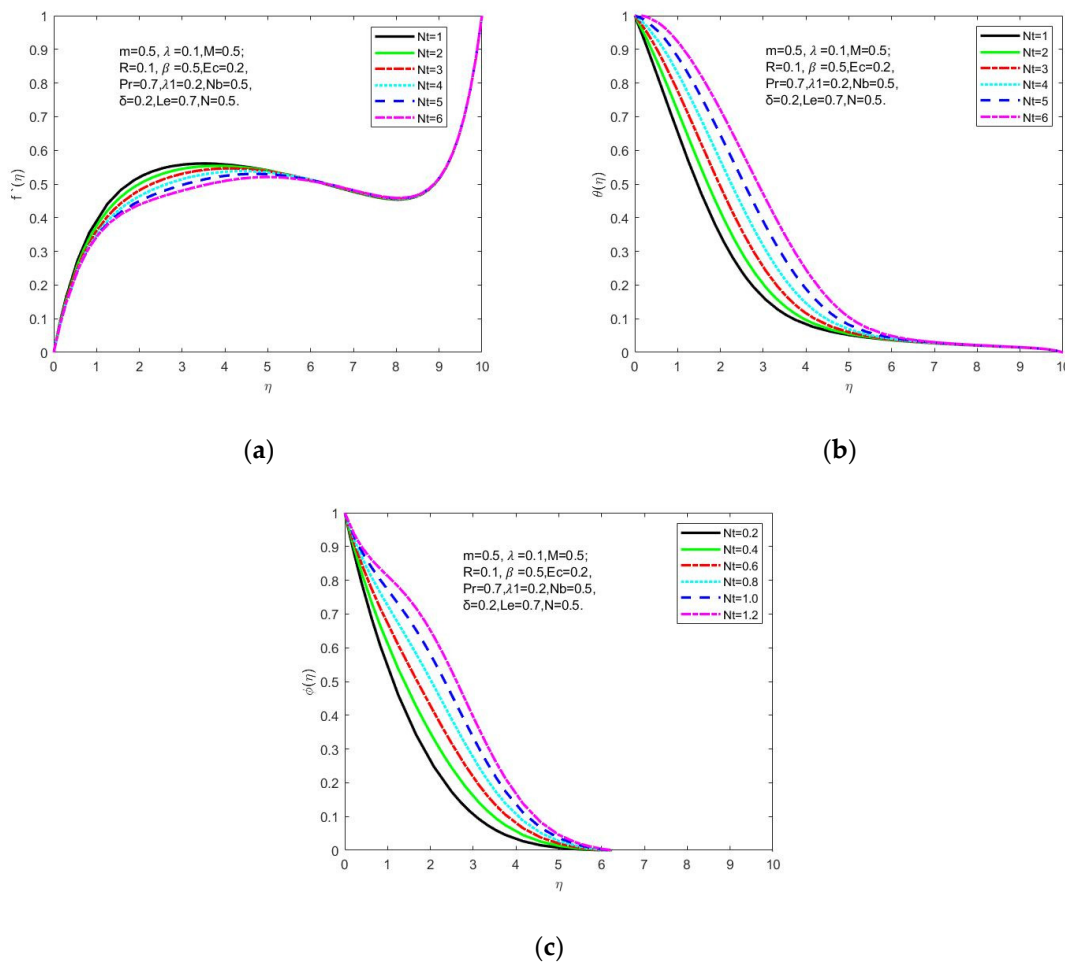


Figure 10. (a) f' vs. N_t , (b) θ vs. N_t , and (c) Φ vs. N_t .

4.10. Impact of R on Velocity, Concentration, and Temperature Patterns of the Nanofluids

As seen in Figure 11a, a rise in R causes a rise in the fluid temperature. This is because a higher value of R heats the working fluid more thoroughly inside the boundary layer area. Figure 11b demonstrates that when R rises, so does the concentration of nanoparticles. However, when R is raised, the nanofluid’s velocity falls (See Figure 11c).

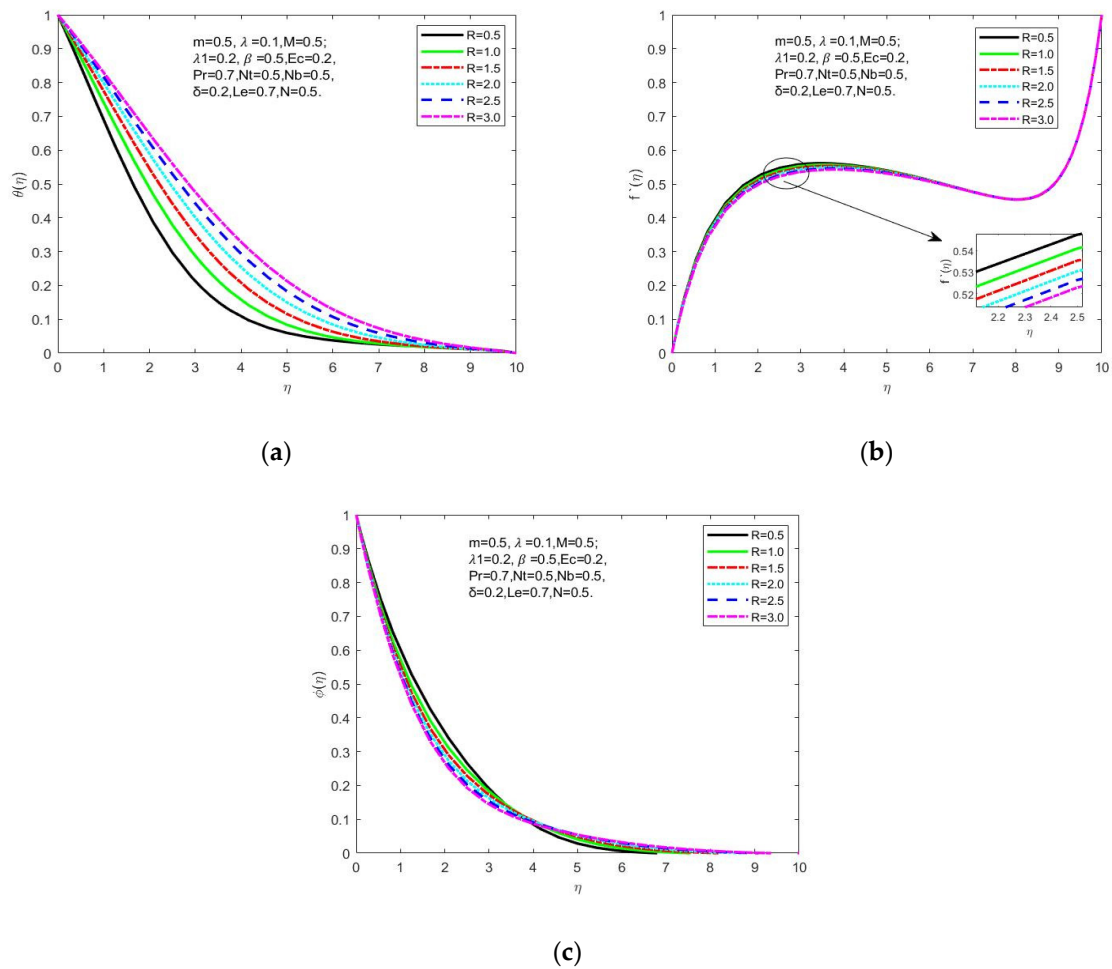


Figure 11. (a) θ vs. R , (b) Φ vs. R , and (c) f' vs. R .

4.11. Impact of λ on Concentration, Fluid Velocity, and Temperature Patterns of the Nanofluids

Figure 12a shows the variation of λ on nanofluid concentration of the nanofluids. As can be observed, Φ lowers as λ grows. This is because the nanofluid has a greater viscosity, which raises its concentration. As a result, the nanofluid's velocity drops due to its increased viscosity, which is shown in Figure 12b. Hence the temperature of the nanofluid increases due to a greater accumulation of heat inside the nanofluids Figure 12c.

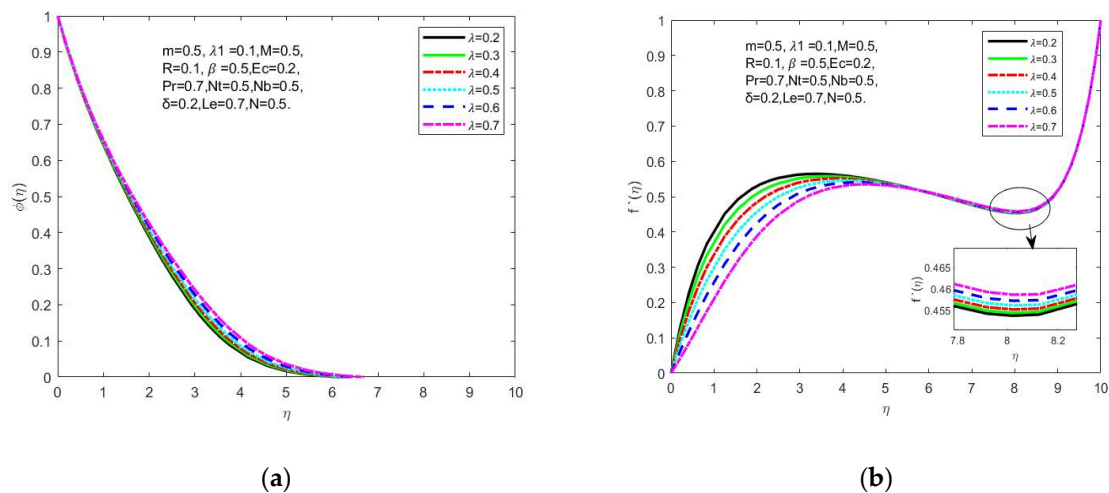
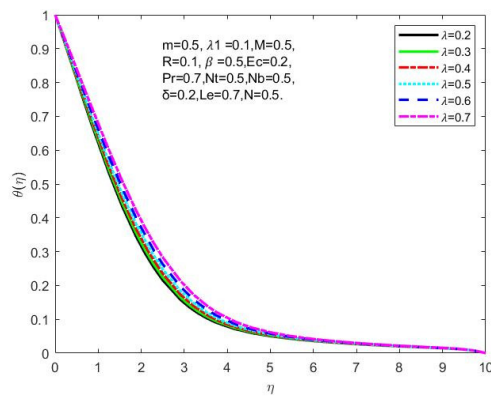


Figure 12. Cont.

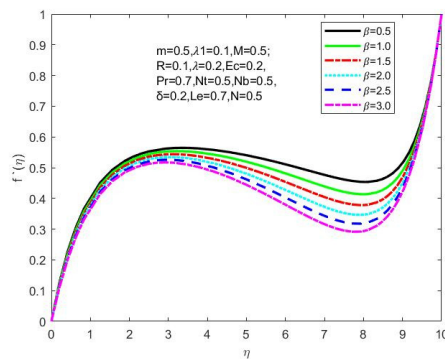


(c)

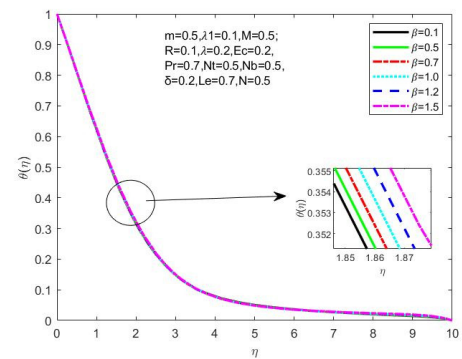
Figure 12. (a) f' vs. λ , (b) θ vs. λ , and (c) Φ vs. λ .

4.12. Influence of β on Fluid Velocity, Concentration, and Temperature Patterns of the Nanofluids

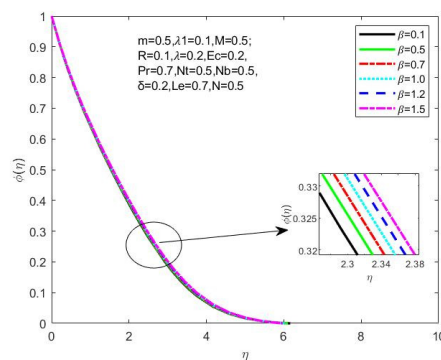
Variations in the velocity profile exposed to the Deborah number (β) are shown in Figure 13a. For Lower β , material was shown to behave in a more fluid-like manner, with an associated Newtonian fluid. For a larger β , on the other hand, the fluid exhibits material behavior as a non-Newtonian regime that is gradually controlled by elasticity, similar to that of a solid. The impact of the β value on the temperature contour is seen in Figure 13b. It is apparent that with increasing values of the Deborah number, a rising behavior in the temperature profile manifests itself. Similar behavior was seen for nanofluid concentration profiles in Figure 13c.



(a)



(b)



(c)

Figure 13. (a) f' vs. β , (b) θ vs. β , and (c) Φ vs. β .

Table 1 compares the local Sherwood number and Nusselt number for increasing m and it is very obvious that the findings of this investigation are compatible with work by Gaffar et al. [15].

Table 1. Comparative study of N_{u_x} and Sh_x for different m values (for $R = 2, \lambda_1 = 0.1, M = 0.5, E_c = 0.2, \beta = 0.5, N_t = 0.5, N_b = 0.5, L_e = 0.7, N = 0.5, Pr = 0.7, \delta = 0.2, \lambda = 0.2$).

m	Gaffar et al. [15]		Current Study	
	N_{u_x}	Sh_x	N_{u_x}	Sh_x
0.1	0.2083	0.3126	0.2292	0.3301
0.2	0.2122	0.3261	0.2362	0.3417
0.3	0.2162	0.3398	0.2376	0.3508
0.4	0.2202	0.3531	0.2426	0.3692

Table 2 displays the results of raising $m, N, Pr, \lambda, \delta$ on HT and mass transfer.

Table 2. N_{u_x} and Sh_x for various values of m, N, Pr, λ and δ (for $R = 2, \lambda_1 = 0.1, M = 0.5, E_c = 0.2, N_t = 0.5, N_b = 0.5, L_e = 0.7$).

m	N	Pr	λ	δ	β	N_{u_x}	Sh_x	
0.1	0.1	0.7	0.2	0.2	0.5	0.2292	0.3301	
						0.2302	0.3322	
						0.2317	0.3348	
	0.5	0.7	0.2	0.2	0.5	0.2302	0.3322	
						0.2455	0.3318	
						0.2571	0.3309	
	0.1	0.7	0.2	0.3	0.2	0.5	0.2292	0.3301
				0.5			0.2340	0.3605
				0.2399			0.3723	
	0.1	0.7	0.2	0.2	0.0	0.5	0.2684	0.3092
					0.2		0.2292	0.3301
					0.4		0.1896	0.6527
0.1	0.5	0.7	0.2	0.2	0.5	0.2302	0.3322	
					0.7	0.2293	0.3213	
					1.0	0.2267	0.3124	

Heat and mass transport rates are seen to significantly increase as λ increases. Furthermore, an increment in N improves the mass and heat transmission rates. Additionally, a rise in Pr is seen to enhance the HT rate while decreasing the mass transfer rate. Likewise, increasing β slows down both HT and mass transfer rates. The mass transfer rate upsurges as δ increases, while the heat transfer rate is noticeably reduced.

5. Conclusions

The analysis of Jeffery nanofluid thermally radiative convective flow over a stretching wedge with viscous dissipation was studied in the current work. The effects of the wedge angle parameter, the NC, R, heat generation, and other parameters are graphically depicted. For a number of physical parameters, the numerical values of the HT and mass transfer are provided, and significant features are thoroughly explained. To validate the present analysis, the mathematical findings are compared to data that have already been

published in the literature while taking into consideration the specific circumstances. It is demonstrated that there is perfect agreement between the two sets of results. A summary of the key findings is as follows:

1. The fluid velocity reduces due to the higher range of radiation and Eckert number parameters;
2. The augmentation in the Prandtl number leads to the improvement in velocity; at the same time, it shows the decreasing phenomena in temperature and nanoparticle concentration field;
3. The temperature field is an increasing function of the mixed convection and buoyancy ratio parameters;
4. An increment in Brownian motion and the Eckert number parameters results in a decrement in the nanoparticle concentration field.

Author Contributions: Conceptualization, Y.D. and K.L.; methodology, R.J.; software, Y.D.; validation, R.J., N.A. and V.R.D.; formal analysis, V.R.D.; investigation, N.A.; resources, A.R.K.; data curation, N.A.; writing—original draft preparation, Y.D. and K.L.; writing—review and editing, K.L. and N.A.; visualization, A.R.K.; supervision, R.J.; project administration, N.A.; funding acquisition, N.A. All authors have read and agreed to the published version of the manuscript.

Funding: Princess Nourah Bint Abdulrahman University Researchers supporting Project number (PNURSP2023R59), Princess Nourah Bint Abdulrahman University, Riyadh, Saudi Arabia.

Data Availability Statement: Not applicable.

Acknowledgments: Princess Nourah Bint Abdulrahman University Researchers supporting Project number (PNURSP2023R59), Princess Nourah Bint Abdulrahman University, Riyadh, Saudi Arabia.

Conflicts of Interest: The authors declare no conflict of interest.

Abbreviations

List of Symbols

Nomenclature

B_0	Magnetic field strength
C	Concentration
C_∞	Ambient concentration
C_w	Sheet concentration
T	Fluid temperature
T_w	Sheet temperature
T_∞	Ambient fluid temperature
D_B	Coefficient of Brownian diffusion
D_T	Coefficient of Thermophoretic diffusion
E_c	Eckert number
k	Thermal conductivity
L_e	Lewis parameter
m	Pressure gradient parameter
M	Magnetic field parameter
N	Concentration to thermal buoyancy ratio parameter
N_b	Brownian diffusion parameter
N_t	Thermophoresis parameter
P_r	Prandtl number
q_r	Radiative heat flux
R	Radiation parameter
λ_2	Relaxation time
λ_1	Ratio of relaxation and retardation time
u, v	Velocity components
x, y	Cartesian coordinates

G_{rx}	Local Grashof number
α_f	Thermal diffusivity
β	Coefficient of thermal expansion
β^*	Coefficient of concentration expansion
β_1	Wedge angle parameter
δ	Heat source/sink parameter
η	Similarity parameter
θ	Temperature similarity function
ϕ	Concentration similarity function
λ	Mixed convection parameter
θ	Kinematic viscosity
ρ	Density
τ	Ratio of the effective heat capacity
σ	Electrical conductivity

References

- Shahzad, F.; Baleanu, D.; Jamshed, W.; Nisar, K.S.; Eid, M.R.; Safdar, R.; Ismail, K.A. Flow and heat transport phenomenon for dynamics of Jeffrey nanofluid past stretchable sheet subject to Lorentz force and dissipation effects. *Sci. Rep.* **2021**, *11*, 1–15. [[CrossRef](#)] [[PubMed](#)]
- Ur Rasheed, H.; AL-Zubaidi, A.; Islam, S.; Saleem, S.; Khan, Z.; Khan, W. Effects of Joule heating and viscous dissipation on magnetohydrodynamic boundary layer flow of Jeffrey nanofluid over a vertically stretching cylinder. *Coatings* **2021**, *11*, 353. [[CrossRef](#)]
- Abdullah Mohamed, R.; Mahmoud Aly, A.; Elsayed Ahmed, S.; Sayed Soliman, M. MHD Jeffrey NanoFluids Flow Over a Stretching Sheet Through a Porous Medium in Presence of Nonlinear Thermal Radiation and Heat Generation/Absorption. *Chall. Nano Micro Scale Sci. Technol.* **2020**, *8*, 9–22.
- Mohamed, R.A.; Ahmed, S.E.; Aly, A.M.; Chamkha, A.J.; Soliman, M.S. MHD Casson nanofluid flow over a stretching surface embedded in a porous medium effect of thermal radiation and slop conditions. *Lat. Am. Appl. Res.* **2021**, *51*, 229–239.
- Al-Kouz, W.; Owhaib, W. Numerical analysis of Casson nanofluid three-dimensional flow over a rotating frame exposed to a prescribed heat flux with viscous heating. *Sci. Rep.* **2022**, *12*, 4256. [[CrossRef](#)] [[PubMed](#)]
- Patil, V.S.; Humane, P.P.; Patil, A.B. MHD Williamson nanofluid flow past a permeable stretching sheet with thermal radiation and chemical reaction. *Int. J. Model. Simul.* **2022**, 1–15. [[CrossRef](#)]
- Abdal, S.; Siddique, I.; Alrowaili, D.; Al-Mdallal, Q.; Hussain, S. Exploring the magnetohydrodynamic stretched flow of Williamson Maxwell nanofluid through porous matrix over a permeated sheet with bioconvection and activation energy. *Sci. Rep.* **2022**, *12*, 278. [[CrossRef](#)]
- Abbas, A.; Jeelani, M.B.; Alnahdi, A.S.; Ilyas, A. MHD Williamson Nanofluid Fluid Flow and Heat Transfer Past a Non-Linear Stretching Sheet Implanted in a Porous Medium: Effects of Heat Generation and Viscous Dissipation. *Processes* **2022**, *10*, 1221. [[CrossRef](#)]
- Loganathan, K.; Rajan, S. An entropy approach of Williamson nanofluid flow with Joule heating and zero nanoparticle mass flux. *J. Therm. Anal. Calorim.* **2020**, *141*, 2599–2612. [[CrossRef](#)]
- Jeffreys, H. *The Earth*, 4th ed.; Cambridge University Press: London, UK, 1929.
- Bird, R.B.; Armstrong, R.C.; Hassager, O. Dynamics of polymeric liquids. In *Fluid Dynamics*, 2nd ed.; Wiley: New York, NY, USA, 1987; Volume 1.
- Nadeem, S.; Akbar, N.S. Peristaltic flow of a Jeffery fluid with variable viscosity in an asymmetric channel. *Z. Für Nat. A* **2009**, *64a*, 713–722. [[CrossRef](#)]
- Hayat, T.; Shehzad, S.A.; Qasim, M.; Obaidat, S. Radiative flow of Jeffery fluid in a porous medium with power law heat flux and heat source. *NuclEng. Des.* **2012**, *243*, 15–19. [[CrossRef](#)]
- Prasad, V.R.; Gaffar, S.A.; Keshava Reddy, E.; Anwar Be'g, O. Flow and heat transfer of Jeffrey's non-Newtonian fluid from horizontal circular cylinder. *J. Thermophys Heat Transfer.* **2014**, *28*, 764–770. [[CrossRef](#)]
- Abdul Gaffar, S.; Ramachandra Prasad, V.; Keshava Reddy, E. Mixed convection boundary layer flows of a non-Newtonian Jeffrey's fluid from a non-isothermal wedge. *Ain Shams Eng. J.* **2017**, *8*, 145–162. [[CrossRef](#)]
- Prasad, V.R.; Gaffar, S.A.; Keshava Reddy, E.; Anwar Beg', O. Numerical study of non-Newtonian boundary layer flow of Jeffrey fluid past a vertical porous plate in a non-Darcy porous medium. *Int. J. Comput. Methods Eng. Sci. Mech.* **2014**, *15*, 372–389. [[CrossRef](#)]
- Ara, A.; Khan, N.A.; Khan, H.; Sultan, F. Radiation effects on boundary layer flow of an Eyring–Powell fluid over an exponentially shrinking sheet. *Ain Shams Eng. J.* **2014**, *5*, 1337–1342. [[CrossRef](#)]
- Noor, N.F.; Abbasbandy, S.; Hashim, I. Heat and mass transfer of thermophoretic MHD flow over an inclined radiate isothermal permeable surface in the presence of heat source/sink. *Int. J. Heat Mass Transf.* **2012**, *5*, 2122–2128. [[CrossRef](#)]
- Gupta, D.; Kumar, L.; Be'g, O.A.; Singh, B. Finite element simulation of mixed convection flow of micropolar fluid over a shrinking sheet with thermal radiation. *Proc. IChemE-Part E J. Process. Mech. Eng.* **2012**, *228*, 61–72. [[CrossRef](#)]

20. Shahid, A.; Bhatti, M.M.; Ellahi, R.; Mekheimer, K.S. Numerical experiment to examine activation energy and bi-convection Carreau nanofluid flow on an upper paraboloid porous surface: Application in solar energy. *Sustain. Energy Technol. Assess.* **2022**, *52*, 102029. [[CrossRef](#)]
21. Bhargava, R.; Sharma, R.; Be'g, O.A. A numerical solution for the effect of radiation on micropolar flow and heat transfer past a horizontal stretching sheet through a porous medium. In Proceedings of the 7th SWEAS International Conference on Heat Mass Transfer (HMT'10), Cambridge, UK, 23–25 February 2010; University of Cambridge: Cambridge, UK, 2010; pp. 88–96.
22. Rosenhead, L. *Laminar Boundary Layers*; Oxford: Cambridge, UK, 1963.
23. Cebeci, T.; Keller, H.B. Shooting and parallel shooting methods for solving the Falkner–Skan boundary-layer equation. *J. Comput. Phys.* **1971**, *7*, 289–300. [[CrossRef](#)]
24. Peddieson, J. Wedge and cone flows of viscoelastic liquids. *AIChE J.* **1973**, *19*, 377–379. [[CrossRef](#)]
25. Sparrow, E.M.; Eichhorn, R.; Gregg, J.L. Combined forced and free convection in boundary layer flow. *Phys. Fluids* **1959**, *2*, 319–328. [[CrossRef](#)]
26. Watanabe, T.; Funazaki, K.; Taniguchi, H. Theoretical analysis on mixed convection boundary layer flow over a wedge with uniform suction or injection. *Acta Mech.* **1994**, *105*, 133–411. [[CrossRef](#)]
27. Kafoussias, N.G.; Nanousis, N.D. Magneto-hydrodynamic laminar boundary layer flow over a wedge with suction or injection. *Can. J. Phys.* **1997**, *75*, 733–742. [[CrossRef](#)]
28. Nanousis, N.D. Theoretical magneto hydrodynamics analysis of mixed convection boundary layer flow over a wedge with uniform suction or injection. *Acta Mech.* **1999**, *138*, 21–30. [[CrossRef](#)]
29. Gorla, R.S.R. Unsteady heat transfer in laminar non-Newtonian boundary layer over a wedge. *AIChE J.* **1982**, *28*, 56–60. [[CrossRef](#)]
30. Yih, K.A. Radiation effects on mixed convection over an isothermal wedge in the porous media: The entire regime. *Heat Transf. Eng.* **2001**, *22*, 26–32. [[CrossRef](#)]
31. Rashidi, M.M.; Rastegari, M.T.; Asadi, M.; Anwar Be'g, O. A study of non-Newtonian flow and heat transfer over a non-isothermal wedge using the homotopy analysis method. *Chem. Eng. Commun.* **2012**, *199*, 231–256. [[CrossRef](#)]
32. Chamkha, A.J.; Mujtaba, M.; Quadri, A.; Issa, C. Thermal radiation effects on MHD forced convection flow adjacent to a non-isothermal wedge in the presence of a heat source or sink. *Heat Mass Transf.* **2003**, *39*, 305–312. [[CrossRef](#)]
33. Hsiao, K.L. MHD mixed convection for viscoelastic fluid past a porous wedge. *Int. J. Non-Linear Mech.* **2011**, *46*, 1–8. [[CrossRef](#)]
34. Ishak, A.; Nazar, R.; Pop, I. Moving wedge and flat plate in a power law fluid. *Int. J. Non-Linear Mech.* **2011**, *46*, 1017–1021. [[CrossRef](#)]
35. Dadhich, Y.; Jain, R.; Gyeltshen, S. Insights of Heat and Mass Transfer in Magneto-Mixed Convective Sisko Nanofluid over a Wedge with Viscous Dissipation. *Math. Probl. Eng.* **2022**, *2022*, 3091897. [[CrossRef](#)]
36. Khan, M.; Sardar, H. On steady two-dimensional Carreau fluid flow over a wedge in the presence of infinite shear rate viscosity. *Results Phys.* **2018**, *8*, 516–523. [[CrossRef](#)]
37. Prabakaran, R.; Eswaramoorthi, S.; Loganathan, K.; Sarris, I.E. Investigation on thermally radiative mixed convective flow of carbon nanotubes/Al₂O₃ nanofluid in water past a stretching plate with joule heating and viscous dissipation. *Micromachines* **2022**, *13*, 1424. [[CrossRef](#)]
38. Du, J.; Wang, R.; Zhuo, Q.; Yuan, W. Heat transfer enhancement of Fe₃O₄-water nanofluid by the thermo-magnetic convection and thermophoretic effect. *Int. J. Energy Res.* **2022**, *46*, 9521–9532. [[CrossRef](#)]
39. Wang, R.; Chen, T.; Qi, J.; Du, J.; Pan, G.; Huang, L. Investigation on the heat transfer enhancement by nanofluid under electric field considering electrophoretic and thermophoretic effect. *Case Stud. Therm. Eng.* **2021**, *28*, 101498. [[CrossRef](#)]
40. Sharma, B.K.; Nidhish, K.M.; Mekheimer, K.S. Combined effect of thermophoresis and Brownian motion on MHD mixed convective flow over an inclined stretching surface with radiation and chemical reaction. *Int. J. Mod. Phys. B* **2022**. [[CrossRef](#)]
41. Ajeeb, W.; da Silva, R.R.S.T.; Murshed, S.M.S. Experimental investigation of heat transfer performance of Al₂O₃ nanofluids in a compact plate heat exchanger. *Appl. Therm. Eng.* **2023**, *218*, 119321. [[CrossRef](#)]
42. Botmart, T.; Sabir, Z.; Raja, M.A.Z.; Weera, W.; Sadat, R.; Ali, M.R. Stochastic procedures to solve the nonlinear mass and heat transfer model of Williamson nanofluid past over a stretching sheet. *Ann. Nucl. Energy.* **2023**, *181*, 109564. [[CrossRef](#)]
43. Ma, H.; He, B.; Su, L.; He, D. Heat transfer enhancement of nanofluid flow at the entry region of microtubes. *Int. J. Therm. Sci.* **2023**, *184*, 107944. [[CrossRef](#)]
44. Pazarlioğlu, H.K.; Ekiciler, R.; Arslan, K.; Mohammed, N.A.M. Exergetic, Energetic, and entropy production evaluations of parabolic trough collector retrofitted with elliptical dimpled receiver tube filled with hybrid nanofluid. *Appl. Therm. Eng.* **2023**, *223*, 120004. [[CrossRef](#)]
45. Sturdza, P. An Aerodynamic Design Method for Supersonic Natural Laminar Flow Aircraft. Ph.D. Thesis, Department Aeronautics and Astronautics, Stanford University, Stanford, CA, USA, December 2003.

Disclaimer/Publisher's Note: The statements, opinions and data contained in all publications are solely those of the individual author(s) and contributor(s) and not of MDPI and/or the editor(s). MDPI and/or the editor(s) disclaim responsibility for any injury to people or property resulting from any ideas, methods, instructions or products referred to in the content.